Soft Matter

Sculpting the Shapes of Giant Unilamellar Vesicles using Isotropic-Nematic-Isotropic Phase Cycles

Journal:	*Soft Matter*
Manuscript ID	SM-ART-06-2021-000910.R1
Article Type:	Paper
Date Submitted by the Author:	31-Aug-2021
Complete List of Authors:	Jani, Purvil; Cornell University, Chemical and Biomolecular Engineering Nayani, Karthik; University of Arkansas Fayetteville, Chemical Engineering Abbott, Nicholas; Cornell University, Chemical and Biomolecular Engineering

Soft Matter

RESEARCH ARTICLE

Cite this: DOI: 10.1039/a9f01194L

Sculpting the Shapes of Giant Unilamellar Vesicles using Isotropic-Nematic-Isotropic Phase Cycles

Purvil Jani[a], Karthik Nayani[b] and Nicholas L. Abbott*[a]

Received XY[th] May 2021

Accepted XY[th] June 2021

rsc.li/soft-matter-journal

Understanding how soft matter deforms in response to mechanical interactions is central to the design of functional synthetic materials as well as elucidation of the behaviors of biological assemblies. Here we explore how cycles of thermally induced transitions between nematic (N) and isotropic (I) phases can be used to exert cyclical elastic stresses on dispersions of giant unilamellar vesicles (GUVs) and thereby evolve GUV shape and properties. The measurements were enabled by the finding that I-N-I phase transitions of the lyotropic chromonic liquid crystal disodium cromoglycate, when conducted via an intermediate columnar (M) phase, minimized transport of GUVs on phase fronts to confining surfaces. Whereas I to N phase transitions strained spherical GUVs into spindle-like shapes, with an efflux of GUV internal volume, subsequent N to I transitions generated a range of complex GUV shapes, including stomatocyte, pear- and dumbbell-like shapes that depended on the extent of strain in the N phase. The highest strained GUVs were observed to form buds (daughter vesicles) that we show, via a cycle of I-N-I-N phase transitions, are connected via a neck to the parent vesicle. Additional experiments established that changes in elasticity of the phase surrounding the GUVs and not thermal expansion of membranes were responsible for the shape transitions, and that I-N-I transformations that generate stomatocytes can be understood from the Bilayer-Coupling model of GUV shapes. Overall, these observations advance our understanding of how LC elastic stresses can be regulated to evolve the shapes of soft biological assemblies as well as provide new approaches for engineering synthetic soft matter.

I. Introduction

Biological cells, vesicles and organelles exhibit diverse membrane morphologies that play key roles in their functions [1, 2]. The biconcave shapes of red blood cells, for example, allow them to move through narrow capillaries to provide efficient oxygen transport [3] and microvilli of epithelial cells create large membrane surface areas for absorption of micronutrients [4]. Cell membranes also undergo dynamic shape transformations that reflect mechanical interactions with the underlying cytoskeleton, and give rise to cellular functions such as cell locomotion, cell division or exo- and endocytosis [5, 6]. To elucidate the design principles evolved in biological systems to achieve these functions, lipid vesicles have been widely explored as simplified and synthetic model systems [7-10]. Past studies have reported on changes in the morphology of lipid vesicles that are induced by changes in temperature [11], osmotic pressure [12-18], optical forces [19-22], pH [23] and hydrodynamic forces [24]. In this study, we go beyond these prior approaches to explore the use of elastic stresses generated by nematic liquid crystals (LCs) to control the evolution of shapes exhibited by giant unilamellar vesicles (GUVs).

Liquid crystalline phases combine the mobility of liquids with the long-range orientational ordering of crystalline solids [25]. Our study uses a class of LCs called lyotropic chromonic phases, which are formed from sheet-like molecules that stack in water into nanoscopic columns (Fig 1A). Fig. 1B shows the structure of disodium cromoglycate (DSCG), the molecule used in our study, with a poly-aromatic core and peripherical carboxylic acid groups. At room temperature and concentrations between ~12% w/w and ~24.5% w/w, the nanoscopic assemblies formed by DSCG organize into the orientationally ordered nematic phase ((N), oriented along the 'director', Fig. 1A). In contrast, for

[a] School of Chemical and Biomolecular Engineering, Cornell University, Ithaca, NY, USA.
[b] Department of Chemical Engineering, University of Arkansas, Fayetteville, AR, USA.
* Corresponding author. Email: nabbott@cornell.edu

†Electronic Supplementary Information (ESI) available. See DOI: 10.1039/a9f01194L

Soft Matter

RESEARCH ARTICLE

concentrations above 24.5% w/w, the columns pack into a hexagonal array with both orientational and positional ordering (forming a columnar phase, M, Fig. 1A). Because both the N and M phases possess long range order, elastic energy can be stored in strained states of these phases at rest. For example, the introduction of microparticles into LCs deforms the LC director and the resultant LC strain leads to a range of interesting phenomena, including chaining and crystallization of colloidal particles [26]. Whereas the inclusions used in most past studies have been 'hard' relative to the LC (i.e., the LC host deforms but the inclusion does not), we have reported that when soft colloids such as synthetic giant unilamellar vesicles (GUVs) [27] or red blood cells [28] are dispersed in nematic LC, the strain is shared both by the LC and the inclusion.

Our study builds from the prior observation that it is possible to disperse GUVs in 15% w/w aqueous DSCG without destruction of the lipid bilayers of the GUVs [27]. This occurs because DSCG molecules are not amphiphilic, in contrast to the majority of other molecules (e.g., surfactants) that form lyotropic LC phases. Previously we found that spherical GUVs formed in isotropic (I) solutions of DSCG (at elevated temperature) were strained into spindle-like shapes when the DSCG solution was cooled into the nematic phase (Fig. 1D, E), due to elastic forces generated by deformation of LC director within and around the GUVs. In particular, large GUVs (surface area > 500 μm^2) were typically strained weakly (R/r < 1.54, where R is semi-major axis and r is semi-minor axis of the strained shape) whereas small GUVs (surface area < 50 μm^2) adopted highly elongated spindle-shapes (R/r > 1.54) [27]. This size-dependent strain of GUVs was shown to arise from an interplay of elastic deformation energy of the LC, E_{LC}, and the surface energy of the interface between the LC and the GUV membrane, E_S (in contrast, the bending energy of the GUV membrane is negligible in magnitude). Specifically, by minimizing the total free energy, $E = E_{LC} + E_S$, at constant volume (V), it can be shown that [27]

$$\frac{R}{r} \propto V^{-\frac{1}{5}} \qquad \text{[Eq. 1]}$$

Of particular relevance to the investigation reported in this paper, our previous study also revealed that the population of highly strained GUVs experience an efflux of internal DSCG solution volume (via strain-induced transient membrane pore formation) during the isotropic to the nematic phase transition (I→N). This decrease in internal volume, which results in an increase in the surface area-to-volume ratio of the GUVs, leads to the key issue that we address in the study reported in this paper. Specifically, we investigate how the high surface area-to-volume ratio of GUVs in the N phase is accommodated by the GUVs when they are subsequently transferred into an I phase. How the GUVs accommodate the excess surface area after the N→I transition was unknown at the outset of this investigation.

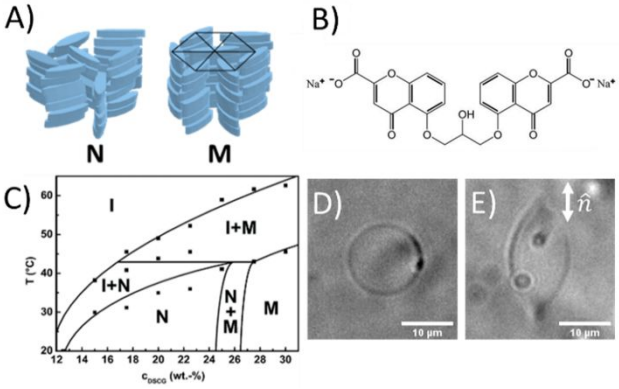

Fig. 1. (A) Schematic illustration of DSCG molecules stacking in the nematic and columnar phases. (B) The chemical structure of DSCG molecule. (C) Temperature – concentration phase diagram of DSCG in water (reproduced from [29] – published by The Royal Society of Chemistry). Bright-field micrographs of GUVs in 15% w/w DSCG at (D) 48°C (isotropic phase) and (E) at 25°C (nematic phase) (Scale bars: 10 µm)

To address the above-described question, we made several advances in methodology for studying GUVs in LCs. First, whereas the methods adopted previously (and described above) for straining GUVs in LCs (a modified method of gentle hydration [30]) led to GUV strain that decreased with increase in size, in this paper, we report a procedure based on electroformation that we show allows generation of GUVs in DSCG that are both large in size (~10-30 µm in diameter) and highly strained. Second, by using high concentrations of DSCG such that the N and I phases are separated by an intermediate M phase, we show that it is possible to avoid transporting GUVs to the surfaces of the sample cells, as often occurs during direct N to I transitions (the GUVs are transported on the phase front to confining surfaces, where GUVs are deformed). Specifically, we show that the M phase of DSCG does not wet the surfaces of the optical cell used to contain samples and thus N→I phase transitions that occur via the intermediate M phase leads to GUVs that remain dispersed in the bulk phase.

Finally, we place our experimental observations into the context of a bilayer-coupling model that describes equilibrium shapes of vesicles based on the membrane surface area, internal volume and difference in area of the

Soft Matter

RESEARCH ARTICLE

internal and external leaflets of the lipid bilayer of a vesicle [31].

II. Methods

Lyotropic LC preparation

Lyotropic LCs containing DSCG were prepared by mixing x % w/w DSCG with $(100 - x)$ % w/w distilled and deionized water, where x is the desired DSCG concentration. Solutions were vortexed and heated (to 70°C) repeatedly until a homogeneous solution was obtained. Solutions of 15% w/w DSCG formed a N phase at room temperature (25°C), and transitioned, via a I + N coexistence region, to an I phase upon increasing the temperature to 48°C. Solutions containing 17% or 18% w/w DSCG solution formed a N phase at room temperature, and transitioned to an I phase via the phase sequence N→I+N→I+M→I upon increasing the temperature to 48°C.

GUV Preparation

We used two methods to prepare GUVs dispersed in solutions of DSCG, as detailed below.

1. **Gentle hydration**

GUVs containing 99 mol % DOPC and 1 mol % DOPE-PEG (2000) were prepared by modifying a previously reported method [30]. In brief, a 100 µL solution of the lipid mixture (total lipid concentration ~ 1 mM) in chloroform was gently dried in a vial using N_2 gas at room temperature to give a film of lipid. The film was further dried under vacuum for at least 2 hours. 2 µL of water was then added to the walls of the vial containing the dried lipid film and the sample was preincubated at 48°C in a water bath for 5 minutes. 200µL of DSCG solution (15% w/w), preheated to 48°C, was then added to the vial and the sample was incubated at 48°C in a water bath for 3 hours. Care was taken to minimize agitation of the vial during incubation. The GUVs so-formed were then diluted 20 times with DSCG solution (15% w/w), at 48°C, before imaging. The samples prepared by this method contained DSCG solution (15% w/w) within and outside the GUVs.

2. **Method of electroformation**

We formed GUVs by electroformation in isotropic DSCG solutions (5% w/w), with a protocol modified from that reported previously to account for the high ionic strength of the DSCG solution [32]. A 10 µL solution of lipid mixture [99 mol % DOPC and 1 mol % DOPE-PEG (2000); total lipid concentration ~ 1 mM] in chloroform was spread on an ITO-coated glass slide (1 cm x 2.5 cm) using a glass microsyringe. The chloroform was then gently dried with N_2 followed by further drying under vacuum for 2 hours. An electroformation chamber was prepared by pairing an ITO-coated glass slide with the lipid-decorated ITO slide, with both separated by a PDMS spacer of thickness 3 mm. The chamber was filled with DSCG solution (5% w/w), and the temperature was maintained at 48°C by using a hotstage. An AC electric field was applied between the two electrodes at 2.6V, 1kHz for 2 hours followed by 1V, 100Hz for 30 minutes. The GUVs were then harvested and cooled to 25°C, before dispersing them in DSCG solutions (nematic phase, 25°C) of higher concentrations (~ 18% w/w) such that the final DSCG concentration of the mixture was 17% w/w.

Preparation of optical cells

We prepared optical chambers from two polyimide-coated glass substrates (rubbed in one direction with a nylon cloth), separated by double-sided tape (~ 100 µm in thickness). The thickness of each optical cell was much larger than the largest GUVs investigated in this study, ensuring that our observations are not influenced by the LC film thickness. GUVs dispersed in aqueous DSCG solution were introduced into each chamber (by capillarity) and the chamber was immediately sealed with vacuum grease to prevent evaporation of water. The rubbed polyimide-coated glass substrates cause planar anchoring of nematic DSCG with an in-plane orientation along the rubbing direction [33].

Materials

1,2-dioleoyl-sn-glycero-3-phosphocholine (DOPC) and 1,2-dioleoyl-sn-glycero-3-phosphoethanolamine-N-[methoxy(polyethylene glycol)-2000] (ammonium salt) (DOPE-PEG 2000) were purchased from Avanti Polar Lipids, Inc. Disodium cromoglycate (DSCG) was purchased from VWR International. ITO-coated slides and chloroform were purchased from Sigma-Aldrich. Distilled water was deionized (resistivity of 18.2 MΩ) using a Milli-Q system (Millipore) and used to prepare all aqueous solutions in the experiments presented in this paper. Polyimide solutions were purchased from HD MicroSystems and were spin-coated on glass slides as per the manufacturer's instructions.

III. Results

Soft Matter

RESEARCH ARTICLE

A. Observations of GUV shape during nucleation of isotropic phase domains

Our initial experiments were performed using GUVs prepared in 15% w/w DSCG solution by the gentle hydration method. In contrast to our previous study that reported on shape changes induced by the I→N phase transition, our initial efforts here focused on characterizing the effects of N→I transitions on GUV shape. We comment first on the behaviors of the GUVs during the nucleation of the I phase from the N phase.

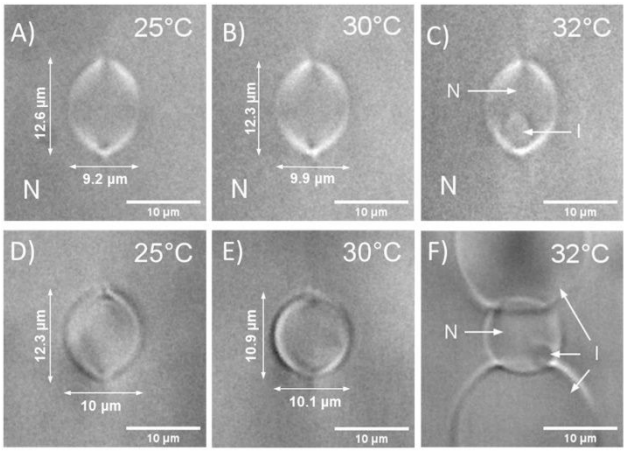

Fig. 2. (A-F) Bright-field micrographs of GUVs in DSCG (15% w/w). (A-B) A GUV in the nematic phase, showing decrease in the aspect ratio (R/r) from (A) 1.36 ± 0.04 at 25°C to (B) 1.25 ± 0.04 at 30°C. (C) Isotropic domain formation (indicated by I) near the surface of the GUV (near the poles/cusp) (D-E) A GUV in the nematic phase, showing decrease in the aspect ratio (R/r) from 1.23 ± 0.04 at (D) 25°C to 1.08 ± 0.04 at (E) 30°C. (F) Isotropic domain formation (indicated by I) near the surface of the GUV. (Scale bars: 10 µm) (the error bars represent uncertainty in measuring the lengths of axes of GUVs from their micrographs)

As described above, the gentle hydration method involves formation of GUVs in 15% w/w DSCG at elevated temperature such that the DSCG solution is an isotropic phase (at 48°C). Consistent with our past report, we observed GUVs that were formed in the isotropic solution of DSCG to be spherical (Fig. 1D). Following a thermal quench to room temperature to form a nematic phase (I→N transition, 25°C), we observed the GUVs to be strained into spindle-like shapes (Fig. 1E) [27]. Interestingly, a further decrease in temperature below 25°C led to an increase in strain of the GUVs and, in some cases, the formation of tubules that extended from the poles of strained GUVs (Fig. S1, ESI †). After straining the GUVs at 25°C, we increased the temperature back to 48°C and imaged the GUVs during the accompanying nematic to isotropic (N→I) phase transition.

Initially, as the temperature within the N phase was increased above 25°C, we observed the strained GUVs to exhibit a decrease in aspect ratio (R/r) (Fig. 2A-B and D-E) (Fig. S2, ESI †). This relaxation of the strained GUV shape is consistent with a decrease in the elastic moduli of DSCG with increasing temperature [34] We note also that DSCG orients tangentially at the GUV membrane and, as reported previously, adopts a twisted configuration at the poles of weakly strained GUVs.[27] With further increase in temperature, we observed isotropic domains to nucleate near the surface of each GUV. In Fig. 2C, the isotropic domain (indicated by 'I') formed near the bottom cusp within the strained GUV, whereas in Fig. 2F, isotropic domains (indicated by 'I') can be seen outside the top and bottom region of the GUV, and on the lower right within the GUV. These observations and others provide evidence of preferential nucleation of the I phase on the GUV surface. Previously, we concluded that there is likely a film of aqueous solution near the surface of each GUV that contains a concentration of DSCG that is lower than the bulk (a depletion layer) [27]. Our results here suggest that this depletion layer of DSCG near the surface of the GUVs serves to nucleate the phase transition of the isotropic phase. Past studies have also reported that isotropic phases tend to nucleate preferentially in regions of high strain and at defects in chromonic LCs [35].

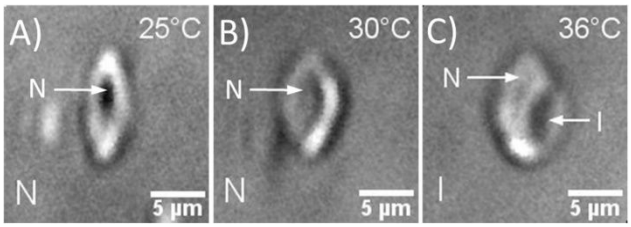

Fig. 3. Bright-field micrographs of a GUV strained in the nematic phase (A) at 25°C and (B) at 30°C. (C) The GUV trapped in an isotropic domain in the coexistence region (at 36°C), showing a strained shape.

In the temperature interval during which the nematic and isotropic phases coexisted, we observed some GUVs to be engulfed outside by I domains while encapsulating N domains within their interiors. In Fig. 3, one such observation is shown. Fig. 3A shows a strained GUV in the nematic phase at 25°C, with an aspect ratio that decreases with increase in temperature to 30°C (Fig. 3B). With further increase of temperature, the GUV is surrounded by an

Soft Matter

RESEARCH ARTICLE

isotropic phase (Fig. 3C). Interestingly, although these trapped GUVs were engulfed by isotropic DSCG phases, they maintained nematic phases within their interiors and exhibited strained shapes. The observation of the strained GUV shape with a nematic interior suggests that the shapes of these GUVs continue to be determined by the elasticity of the encapsulated N phase (Section 3, ESI †). This observation is consistent with a past report in which GUVs encapsulating aqueous DSCG solution were prepared by a double emulsion method [36].

B. GUV shape after the N to I transition

Next, we consider the shapes of GUVs after completion of the N→I transition. We organize our observations according to whether the GUVs were large and weakly strained (R/r < 1.54) or small and highly strained (R/r > 1.54) in the N phase prior to the N→I transition, as discussed in the Introduction [27].

Weakly strained GUVs (R/r <1.54): For large GUVs that are weakly strained in the nematic LC phase (see Eq. 1), there is no change in internal volume during the initial I to N phase transition [27]. Moreover, because the GUVs are prepared at 48 °C (isotropic DSCG phase), after cooling to room temperature (25°C) and then heating to 48°C, there is no net thermal expansion/contraction of the GUV membrane. These two points suggest that after a complete I-N-I cycle, for this population of GUVs, there should be no change in the surface area-to-volume ratio and the GUVs should return to their initial spherical shape after the N→I transition. Consistent with this prediction, as shown in Fig. 4A, B, we observed GUVs that were weakly strained (Fig. 4A R/r = 1.49 ± 0.04) in the nematic phase to return to their spherical shapes after the N→I transition.

Highly strained GUVs (R/r > 1.54): As noted earlier, this population of small GUVs experiences a reduction in internal volume during the initial I→N transition, to yield highly elongated shapes [27] (Fig. 4D, G, J). After an I-N-I cycle, since there is no net change in the membrane area, we predicted that the cycle would cause a net increase in the surface area-to-volume ratio of these GUVs. Consistent with this prediction, we observed GUVs in the isotropic phase (after the N→I transition) to possess an excess area (difference between the surface area of the GUV and the surface area of a sphere having the same volume) that resulted in formation of non-spherical shapes that differed from those observed in the N phase (Fig. 4E, H, K).

We found that the shapes exhibited by the GUVs, after the N→I transition, depended on the extent of straining of the GUVs in the nematic phase. For example, as shown in Fig. 4D, a highly strained GUV (R/r = 1.76 ± 0.16) in the N phase, formed a stomatocyte/inside-budded shape (determined based on the two-dimensional projection of the GUV onto the image plane) in the isotropic phase (Fig. 4E). Similarly, a GUV with R/r = 1.79 ± 0.21 (Fig. 4G) in the N phase was observed to adopt a stomatocyte shape (Fig. 4H) in the I phase. Alternatively, a GUV (Fig. 4J) with R/r = 3.42 ± 0.68 in the N phase was observed to form a dumbbell-like shape (Fig. 4K) upon return of the I phase. We discuss these shapes in the context of the bilayer-coupling model in Section C. In addition to the shapes reported above, we also observed more complex shapes and secondary structure formation such as shedding of the GUV membrane area in the form of 'daughter' vesicles. We detail these observations later in this paper.

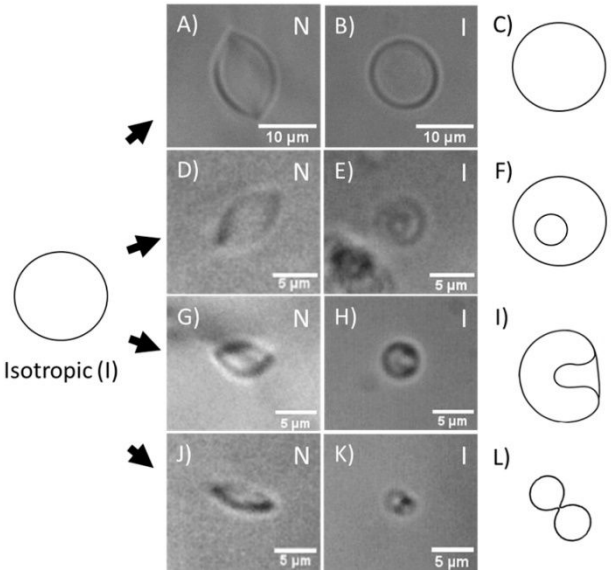

Fig. 4. Bright-field micrographs of GUVs in the (A, D, G, J) nematic phase showing strained shapes and (B, E, H, K) their respective equilibrium shapes in the isotropic phase. (A) A slightly strained GUV in the nematic phase is observed to form a (B) spherical shape in the isotropic phase. (D, G, J) Highly strained GUVs in the nematic phase form (E, H, K) non-spherical shapes in the isotropic phase. (C, F, I, L) Schematic illustration of the observed non-spherical shapes in the isotropic phase (B, E, H, K) respectively. [Values of reduced area difference (Δa), reduced volume (v) (see bilayer-coupling model, below) and aspect ratio (R/r) for the strained GUVs in (D) $\Delta a = 0.94 \pm 0.004$, $v = 0.94 \pm 0.018$, R/r = 1.76 ± 0.16 (G) $\Delta a = 0.94 \pm 0.006$, $v = 0.94 \pm 0.024$, R/r = 1.79 ± 0.21 (J) $\Delta a = 1.02 \pm 0.04$, $v = 0.76 \pm 0.061$, R/r = 3.42 ± 0.68 (the error bars represent uncertainty in measuring the lengths of axes of GUVs from

Soft Matter

RESEARCH ARTICLE

their micrographs)]. Images (E, H, K) were post-processed as described in section 8, ESI †.

The observations reported above using GUVs prepared by the direct hydration method provide evidence that I-N-I phase cycles can be used to mechanically sculpt GUVs into a variety of non-spherical shapes. However, we encountered two challenges when performing the above-described experiments with 15% w/w DSCG in water. Below we detail these challenges and the development of new methods to overcome them.

First, we observed that during the N→I transition (i.e. N → N+I → I) for 15% w/w DSCG solutions, many GUVs in the dispersion were displaced from the bulk of the sample by the moving interface formed between the nematic and isotropic phases. Specifically, the interfacial tension ($\gamma_{NI} \sim 10^{-4}$ J/m^2 [35]) between the two phases (isotropic and nematic) caused the GUVs to adsorb at the interface. We estimated the adsorption energy to be $\gamma_{NI}R^2 \sim 10^{-14}$ J ($\sim 10^7$ kT), consistent with our observation of irreversible adsorption. Furthermore, with increasing temperature, we observed the nematic domains to wet the glass surfaces of the optical cells, causing the GUVs adhered to the I-N interface to be drawn into contact with the surfaces of the optical cell. At the end of the N→I transition, we observed many GUVs to be adhered to the surface and/or burst, thus preventing observation of their shape sculpted by the I-N-I cycle.

During experiments performed to find a solution to the above-described issue (e.g. treatment of the optical cell surface to prevent wetting by the N phase [37]; changing the rates of heating and cooling, etc.), we explored the influence of the DSCG concentration on the phase transition and GUV behavior. Specifically, we used DSCG solutions with a higher concentration (17% w/w) that transitioned from a nematic phase to an isotropic phase via a columnar (M) phase (N → I+N → I+M → I). At this concentration, upon increasing the temperature, the nematic domains in the solution decrease in size, and then transform to columnar domains before forming the isotropic phase. Significantly, during this process, we observed that the GUVs are excluded from M phase domains (the columnar domains also do not wet the glass surfaces).

The accommodation of inclusions (i.e. GUVs) in N phases can be attributed, in part, to the low value of the twist elastic constant (K_{22}) of DSCG [38], making it possible for the LC phase to lower elastic energy through twisting. However, a columnar (M) phase cannot be splayed or twisted without introducing defects/dislocations [39, 40], which we interpret to prevent accommodation of GUVs. The complete exclusion of GUVs from M phases likely also decreases the area of contact of GUVs with M-I interfaces (compared to the area of contact of GUVs with N-I interfaces), causing an apparent decrease in the adsorption energy ($\gamma_{MI}R^2$) (compared to the adsorption energy on N-I interface). Hence, with increasing temperature, when nematic domains convert to columnar domains, the GUVs that are carried by the N-I interface detach from the M-I interface and remain suspended in the bulk isotropic phase. The exclusion of surface functionalized PMMA particles (of diameter ~ 200nm) by the columnar phase has been observed by Zimmermann and coworkers [29].

The second challenge that we encountered when using the gentle hydration method to form GUVs was related to the extent of strain that could be designed into the GUVs in the N phase. As mentioned earlier, GUVs that are highly strained are small in size (Eq. 1) (surface area < 50 μm^2, radius < 2 μm), making it difficult to obtain images that allow unambiguous identification of the shapes of GUVs after the I-N-I cycle. To address this issue, we explored a second approach to formation of strained GUVs in DSCG. We prepared vesicles in DSCG solution (5% w/w) using the method of electroformation at 48°C (see Methods). The method of electroformation is known to generate large GUVs [41]. We then dispersed the electroformed GUVs in a DSCG solution of high concentration (~18% w/w) such that the final concentration of the equilibrated mixture was 17% w/w. Upon dispersing the GUVs in ~18% w/w DSCG solution, the osmotic pressure difference between the interior and exterior of the GUVs was observed to drive a flux of water out of the GUVs until an osmotic balance was reached. Using this method, we obtained large GUVs that were highly strained in the nematic phase of DSCG (Fig. 5A and D). Upon increasing the temperature (from 25°C to 48° C) of these samples, the phases changed in the order: N → I+N → I+M → I. This method allowed us to image a single GUV processed through an entire I-N-I cycle (Fig. S3, ESI †).

Soft Matter

RESEARCH ARTICLE

Fig. 5 shows a series of observations made using our optimized protocols. In particular, when GUVs *of similar size* were compared, we observed GUVs prepared using the optimized protocols to be strained to higher aspect ratios as compared to GUVs formed using the method of gentle hydration (Fig. 4). In our observations shown in Fig. 5, two of the highest strained GUVs in the N phase (Fig. 5A and D having aspect ratios 3.39 ± 0.4 and 2.85 ± 0.41, respectively) were subsequently observed to form outside budded shapes in the I phase, as determined from two-dimensional projections of the GUVs onto the image plane (Fig. 5B and E). For lower extents of straining, we observed GUVs (Fig. 5J) with R/r = 1.80 ± 0.24 in the N phase to form dumbbell-like shapes in the I phase (Fig. 5K) whereas another GUV (Fig. 5G) with R/r = 1.64 + 0.12 in the N phase formed a stomatocyte/inside-budded shape in the I phase (Fig. 5H).

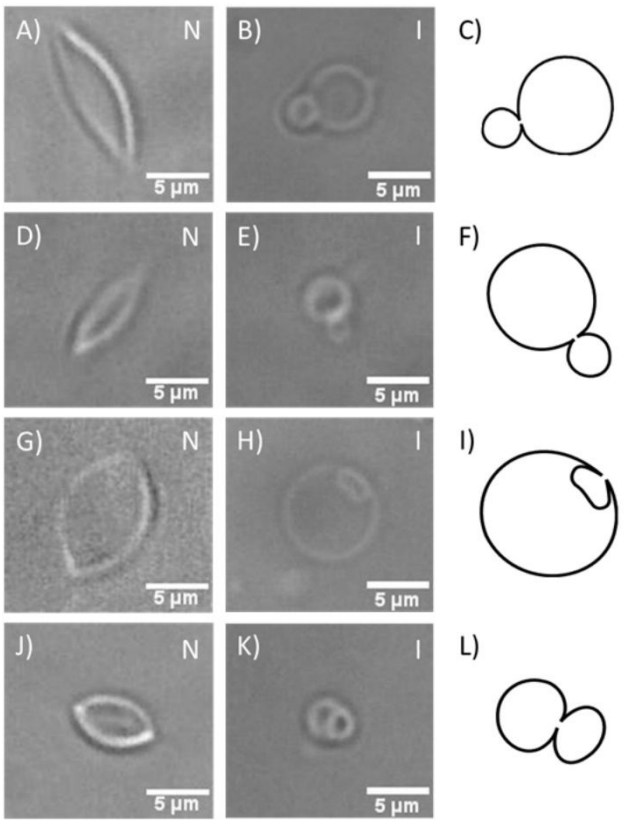

Fig. 5. Bright-field micrographs of GUVs in the (A, D, G and J) nematic phase showing strained shapes and (B, E, H and K) their respective equilibrium shapes in the isotropic phase. (C, F, I and L) Schematic illustration of the observed non-spherical shapes in the isotropic phase (B, E, H and K) respectively. [Values of reduced area difference (Δa), reduced volume (v) (see bilayer-coupling model, below) and aspect ratio (R/r) for the strained GUVs in (A) $\Delta a = 1.02 \pm 0.024$, $v = 0.76 \pm 0.036$, R/r = 3.39 ± 0.4 (D) $\Delta a = 0.99 \pm 0.023$, $v = 0.81 \pm 0.043$, R/r = 2.85 ± 0.41 (G) $\Delta a = 0.94 \pm 0.003$, $v = 0.95 \pm 0.013$, R/r = 1.64 ± 0.12 (J) $\Delta a = 0.94 \pm 0.01$, $v = 0.93 \pm 0.029$, R/r = 1.80 ± 0.24]. (The error bars represent uncertainty in measuring the lengths of axes of GUVs from their micrographs). Images (B, E, H, K) were post-processed as described in section 8, ESI †.

Observations based on multiple I-N-I cycles

The experimental observations described above were based on procedures that involved the use of a single I-N-I cycle to change the shapes of the GUVs. It is possible, however, to subject GUVs to additional cycles of strain by further phase transitions. Here we illustrate the utility of this capability by providing insight into the formation of "buds" from parent vesicles after N→I transitions, as shown by Fig. 5B, E and K.

Specifically, to address the question of whether the buds physically separate from the parent GUVs, we performed experiments in which we observed a single GUV undergoing multiple I-N-I cycles. Fig. 6A shows a GUV that is strained in the N phase (at 25°C) of DSCG (17% w/w) solution. Upon increasing the temperature to 48°C, the GUV was observed to form a dumbbell shape in the I phase (Fig. 6B). Upon quenching the sample to the N phase, we observed the GUV form a single strained vesicle (Fig. 6C) (see Fig. S5, ESI †). This observation supports our conclusion that the buds (in this case, the two lobes of the dumbbell shape) do not physically separate in the I phase and belong to a single GUV. Previous studies of temperature-induced shape transitions of GUVs have also reported that budded parts of a vesicle can remain connected via a narrow neck [11, 12, 42]. The presence of a narrow neck between the two parts of vesicles allows transfer of internal solution volume between them as well as the exchange of lipid molecules across the fluid bilayer of the entire assembly.

Soft Matter

RESEARCH ARTICLE

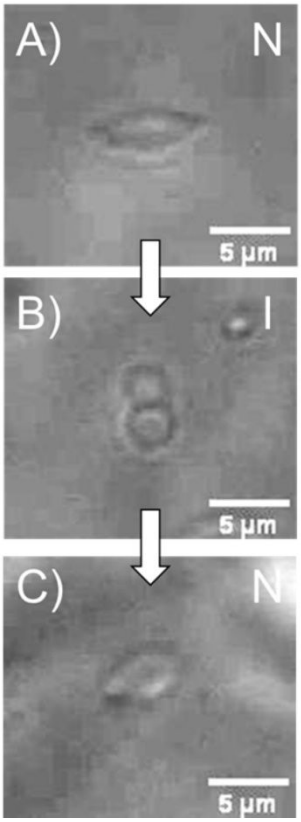

Fig. 6. Bright-field micrographs of a GUV undergoing cycling with temperature changing from (A) 25°C (nematic phase) to (B) 48°C (isotropic phase) to (C) 25°C (nematic phase)

Prior to providing additional discussion of the factors that influence GUV shapes during I-N-I cycles, we address the possibility that the shapes of GUVs in our experiments are affected by thermal expansion or contraction of the lipid bilayer as we use temperature-induced phase transitions to regulate the mechanical forces applied to the GUVs. Specifically, we subjected GUVs to temperature cycles in the absence of LC elastic forces (i.e. in an isotropic phase). We prepared GUVs in 5% w/w DSCG solutions at 48°C. Upon cycling the temperature of the GUV sample from 48°C to 25° C and then back to 48°C at a rate of 5°C/min, we observed the GUVs to remain spherical in shape throughout the entire experiment (Fig. S6, ESI †). This observation suggests that LC elastic stresses, and not thermal expansion/contraction of the membrane, are responsible for GUV shape changes shown in Figures 4, 5 and 6.

C. Bilayer-Coupling Model

Our results in Figures 4, 5 and 6 reveal that a diverse range of non-spherical GUV shapes can be formed by I-N-I cycling. Here, we place these observations into the context of the so-called Bilayer-Coupling (BC) model [31]. A key assumption of this model is that there is no exchange of lipid molecules between the opposing leafs (of the GUV membrane) on experimentally relevant time-scales, thus placing a constraint on the area difference between the two monolayers. Within the framework of this model, the bending energy of the vesicle is evaluated as,

$$G_b = \kappa/2 \oint dA(C_1 + C_2)^2 \ , \qquad \text{[Eq. 3]}$$

where κ is the bending elastic modulus of the bilayer membrane and C_1 and C_2 denote the two principal curvatures. The bending energy, G_b, is then minimized for a given area A, volume V and area difference of the two monolayers ΔA, where

$$\Delta A \equiv A^{ex} - A^{in}, \qquad \text{[Eq. 4]}$$

and A^{ex} and A^{in} are the areas of the exterior and interior monolayers, respectively. ΔA is evaluated from the integrated mean curvature (M) as,

$$\Delta A \approx 2DM \ ; M \equiv \tfrac{1}{2}\oint dA \ (C_1 + C_2), \qquad \text{[Eq. 5]}$$

where D is the distance between the two monolayers (~ 2 nm). The phase diagram of axisymmetric shapes obtained by minimizing G_b is shown in Fig. 7 [43]. In Fig. 7, the dimensionless variables Δa and v denote the reduced area difference and reduced volume, respectively, and are given by,

$$\Delta a \equiv M/(4\pi R_0) \qquad \text{[Eq. 6 (a)]}$$

$$v \equiv V/((4\pi/3)R_0^3) \qquad \text{[Eq. 6 (b)]}$$

where

$$R_0 \equiv \sqrt{\tfrac{A}{4\pi}} \qquad \text{[Eq. 6 (c)]}$$

We calculate the values of Δa and v using equations (6a) and (6b), respectively, for highly strained GUVs observed in the N phase (Section 5, ESI †). These calculations revealed that Δa increased from 0.94 to 1.02, and v varied from 0.75 to 0.95, as R/r increased from 1.6 to 3.5. For the strained GUV shown in Fig. 4G with $R/r = 1.79 \pm 0.21$, and corresponding values of $\Delta a = 0.94 \pm 0.006$ and $v = 0.94 \pm 0.024$, we calculated that the GUV lies in the stomatocyte region in the phase diagram of the BC model (Fig. 7), a result that is consistent with our experimental observation of formation of a stomatocyte shape after the N→I transition (Fig. 4H).

Soft Matter

RESEARCH ARTICLE

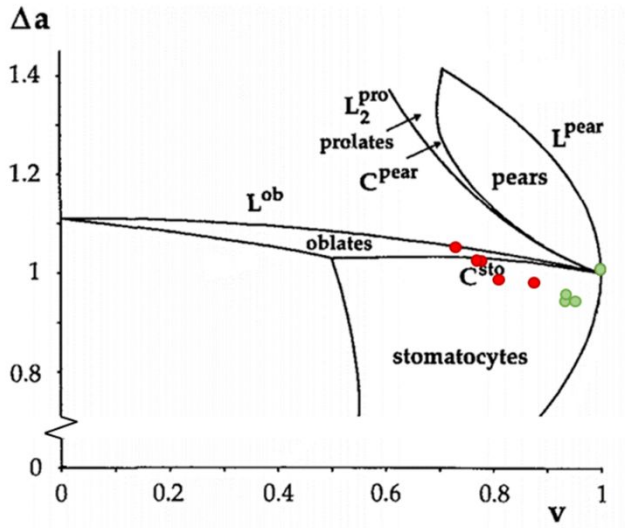

Fig. 7. Phase diagram of the bilayer-coupling (BC) model obtained by minimizing the total bending free energy for a given value of Δa and v. C^{sto} and C^{pear} denote the lines of continuous transitions. L^{pear} and L^{sto} are limit curves that correspond to outside budding and inside budding, respectively. (pro, ob and sto stand for prolates, oblates and stomatocytes, respectively). Green and red dots represent experimentally obtained data points that are in agreement and disagreement with the BC model, respectively. Adapted with permission from [43] - Copyright 1991 by the American Physical Society.

For other GUVs with R/r less than 2 (shown in Fig. 4 and Fig. 5), we calculated v and Δa values and found the BC model to predict stomatocyte shapes, consistent with experiments (Fig. 7) (4 independently prepared GUV samples). However, for higher values of R/r, which correspond to values of $v < 0.94$ and $\Delta a \sim 0.99 - 1.02$, we observed GUVs to form outside budded shapes (Fig. 5B, E) and dumbbell shapes (Fig. 4K and Fig. 5K) after the N→I transition (5 independently prepared GUV samples), a result that is not consistent with the prediction of the BC model. A number of possible reasons may underlie our observation that agreement between the BC model and experimental observation is limited to R/r<2. In particular, the BC model assumes there to be no spontaneous curvature in the GUV membranes, an assumption that may not be accurate for GUVs subjected to extreme strain (e.g., R/r>2). It is possible, for example, that spontaneous curvature in the membrane arises during the efflux of internal solution via transient pores that are formed in membranes of highly strained GUVs during the initial I→N transition [27]. Past studies [44, 45] have shown that the lipid flip-flop rate in a bilayer membrane is increased by the presence of pores. In summary, a comparison of our experimental observations to the BC model hints that dynamical straining of GUVs with LC elastic forces (by I-N-I cycling) may change not only the surface area-to-volume ratio of the GUVs but also introduce changes in GUV membrane properties (such as a spontaneous curvature).

IV. Conclusions

Overall, our study reveals how initially spherical GUVs present in an isotropic phase can be transformed to complex non-spherical shapes by transient exposure to a nematic phase. In particular, we present experimental evidence that I-N-I cycling leads to the transformation of initially spherical vesicles to non-spherical shapes because of a strain-induced reduction of internal volume in the intermediate N phase. We observed the sculpting of initially spherical GUVs into shapes such as stomatocytes, outside-budded and dumbbell shapes by I-N-I phase processing of the GUVs. Additionally, by extending the phase cycling to I-N-I-N, we show that budded vesicles are not disconnected from the parent vesicle but, rather, are connected via a narrow 'neck'. The observation of I-N-I sculpting of GUVs into stomatocytes was found to be consistent with the BC model when the reduced volume and reduced area difference of the GUVs were evaluated in the intermediate N phase. Extreme straining of GUVs, however, led to shapes not predicted by the BC model, suggesting that membrane mechanical properties (e.g., spontaneous curvature) may be changed at high strain.

The conclusions described above were enabled by several experimental advances that we judge to be broadly useful for studies of GUVs. First, we demonstrated that electroformation of GUVs in dilute (isotropic) phases and subsequent dehydration via equilibration with concentrated (nematic) DSCG solutions permits the preparation of large and highly strained GUVs in nematic phases. Second, we found that use of a DSCG concentration that caused the N to I transition to occur via the M phase largely eliminated adsorption of GUVs onto the phase boundary and subsequent transport of the GUVs out of the bulk phase (and onto the surfaces of the sample cell) during the phase transition. Third, by manipulating the temperature of the N phase containing the GUVs, it is possible to tune the extent of strain of GUVs, and thus prescribe a surface area-to-volume ratio in the isotropic phase that plays a key role in determining GUV shape. For example, similar to red blood cells, we envisage shape-controlled GUVs to have potentially advantageous transport properties as they can adapt their shape to access confined geometries (e.g., capillaries). More broadly, LC elastic stresses can be used to strain soft colloids of biological relevance, such as cells and other biologically-derived vesicles, to study their mechanical properties. Other

Soft Matter

RESEARCH ARTICLE

possible directions of future inquiry include tuning of transport properties of lipid membranes under stress, or studying curvature-mediated phase separation in mixed lipid membranes. Our results reported in Fig. 3 also suggest that experimental investigations of GUVs with nematic DSCG present on only one side of the GUV membrane may provide additional insight into GUV shape-responses to LC elastic stresses.

Conflicts of interest

There are no conflicts to declare.

Acknowledgements

The authors acknowledge support from the National Science Foundation (DMR-2003807). Additionally, facilities of the Cornell MRSEC (DMR-1719875) are gratefully acknowledged.

Notes and references

1. A. Prasad and E. Alizadeh, *Trends Biotechnol*, 2019, **37**, 347-357.
2. J. V. Shah, *J Cell Biol*, 2010, **191**, 233-236.
3. W. H. Reinhart and S. Chien, *Blood*, 1986, **67**, 1110-1118.
4. H. F. Helander and L. Fandriks, *Scand J Gastroenterol*, 2014, **49**, 681-689.
5. L. Blanchoin, R. Boujemaa-Paterski, C. Sykes and J. Plastino, *Physiol Rev*, 2014, **94**, 235-263.
6. C. Simon, V. Caorsi, C. Campillo and C. Sykes, *Physical Biology*, 2018, **15**.
7. M. Osawa and H. P. Erickson, *P Natl Acad Sci USA*, 2013, **110**, 11000-11004.
8. A. Upadhyaya, J. R. Chabot, A. Andreeva, A. Samadani and A. van Oudenaarden, *P Natl Acad Sci USA*, 2003, **100**, 4521-4526.
9. J. Nam and M. M. Santore, *Phys Rev Lett*, 2011, **107**, 078101.
10. J. B. Hutchison, A. P. Karunanayake Mudiyanselage, R. M. Weis and A. D. Dinsmore, *Soft Matter*, 2016, **12**, 2465-2472.
11. J. Kas and E. Sackmann, *Biophys J*, 1991, **60**, 825-844.
12. A. Viallat, J. Dalous and M. Abkarian, *Biophys J*, 2004, **86**, 2179-2187.
13. A. L. Bernard, M. A. Guedeau-Boudeville, L. Jullien and J. M. di Meglio, *Biochim Biophys Acta*, 2002, **1567**, 1-5.
14. E. Boroske, M. Elwenspoek and W. Helfrich, *Biophys J*, 1981, **34**, 95-109.
15. J. de Gier, *Chem Phys Lipids*, 1993, **64**, 187-196.
16. K. Koseki and H. Suzuki, *Langmuir*, 2020, **36**, 6238-6244.
17. H. Naito, M. Okuda and O. Y. Zhong-can, *Phys Rev E Stat Phys Plasmas Fluids Relat Interdiscip Topics*, 1996, **54**, 2816-2826.
18. C. Taupin, M. Dvolaitzky and C. Sauterey, *Biochemistry*, 1975, **14**, 4771-4775.
19. E. Spyratou, E. A. Mourelatou, A. Georgopoulos, C. Demetzos, M. Makropoulou and A. A. Serafetinides, *Colloids and Surfaces A: Physicochemical and Engineering Aspects*, 2009, **349**, 35-42.
20. V. N. Georgiev, A. Grafmuller, D. Bleger, S. Hecht, S. Kunstmann, S. Barbirz, R. Lipowsky and R. Dimova, *Adv Sci (Weinh)*, 2018, **5**, 1800432.
21. C. Pernpeintner, J. A. Frank, P. Urban, C. R. Roeske, S. D. Pritzl, D. Trauner and T. Lohmuller, *Langmuir*, 2017, **33**, 4083-4089.
22. D. P. Cherney, T. E. Bridges and J. M. Harris, *Anal Chem*, 2004, **76**, 4920-4928.
23. H. Jia, T. Litschel, M. Heymann, H. Eto, H. G. Franquelim and P. Schwille, *Small*, 2020, **16**, e1906259.
24. G. Coupier, A. Farutin, C. Minetti, T. Podgorski and C. Misbah, *Phys Rev Lett*, 2012, **108**, 178106.
25. P. J. Collings and J. W. G. Goodby, *Introduction to liquid crystals : chemistry and physics*, [Second edition]. edn.
26. I. Musevic, M. Skarabot, U. Tkalec, M. Ravnik and S. Zumer, *Science*, 2006, **313**, 954-958.
27. P. C. Mushenheim, J. S. Pendery, D. B. Weibel, S. E. Spagnolie and N. L. Abbott, *Proc Natl Acad Sci U S A*, 2016, **113**, 5564-5569.
28. K. Nayani, A. A. Evans, S. E. Spagnolie and N. L. Abbott, *Proc Natl Acad Sci U S A*, 2020, **117**, 26083-26090.
29. N. Zimmermann, G. Junnemann-Held, P. J. Collings and H. S. Kitzerow, *Soft Matter*, 2015, **11**, 1547-1553.

Soft Matter

RESEARCH ARTICLE

30. Y. Yamashita, M. Oka, T. Tanaka and M. Yamazaki, *Biochimica Et Biophysica Acta-Biomembranes*, 2002, **1561**, 129-134.
31. S. Svetina and B. Zeks, *Eur Biophys J*, 1989, **17**, 101-111.
32. T. Pott, H. Bouvrais and P. Meleard, *Chem Phys Lipids*, 2008, **154**, 115-119.
33. Y. A. Nastishin, H. Liu, T. Schneider, V. Nazarenko, R. Vasyuta, S. V. Shiyanovskii and O. D. Lavrentovich, *Phys Rev E Stat Nonlin Soft Matter Phys*, 2005, **72**, 041711.
34. S. Zhou, K. Neupane, Y. A. Nastishin, A. R. Baldwin, S. V. Shiyanovskii, O. D. Lavrentovich and S. Sprunt, *Soft Matter*, 2014, **10**, 6571-6581.
35. Y. K. Kim, S. V. Shiyanovskii and O. D. Lavrentovich, *J Phys Condens Matter*, 2013, **25**, 404202.
36. P. Bao, D. A. Paterson, S. A. Peyman, J. C. Jones, J. A. T. Sandoe, H. F. Gleeson, S. D. Evans and R. J. Bushby, *Soft Matter*, 2021, **17**, 2234-2241.
37. H. Lee, V. Sunkara, Y. K. Cho and J. Jeong, *Soft Matter*, 2019, **15**, 6127-6133.
38. A. Nych, U. Ognysta, I. Musevic, D. Sec, M. Ravnik and S. Zumer, *Phys Rev E Stat Nonlin Soft Matter Phys*, 2014, **89**, 062502.
39. P.-G. d. Gennes, *The physics of liquid crystals*, Clarendon Press, Oxford, Repr. with corrections and additions. edn., 1975.
40. M. A. Lohr, M. Cavallaro, Jr., D. A. Beller, K. J. Stebe, R. D. Kamien, P. J. Collings and A. G. Yodh, *Soft Matter*, 2014, **10**, 3477-3484.
41. R. Dimova, S. Aranda, N. Bezlyepkina, V. Nikolov, K. A. Riske and R. Lipowsky, *J Phys Condens Matter*, 2006, **18**, S1151-1176.
42. Y. Li and P. R. Ten Wolde, *Phys Rev Lett*, 2019, **123**, 148003.
43. U. Seifert, K. Berndl and R. Lipowsky, *Phys Rev A*, 1991, **44**, 1182-1202.
44. E. Fattal, S. Nir, R. A. Parente and F. C. Szoka, Jr., *Biochemistry*, 1994, **33**, 6721-6731.
45. D. P. Tieleman and S. J. Marrink, *J Am Chem Soc*, 2006, **128**, 12462-12467.